NJC

ROYAL SOCIETY OF CHEMISTRY

PAPER

View Article Online
View Journal | View Issue

Cite this: *New J. Chem.*, 2020, **44**, 14108

Solid-state host–guest influences on a BODIPY dye hosted within a crystalline sponge†

William J. Gee, *[a] Helena J. Shepherd, [b] Daniel M. Dawson, [c] Sharon E. Ashbrook, [c] Paul R. Raithby [d] and Andrew D. Burrows *[d]

Received 12th June 2020,
Accepted 30th July 2020

DOI: 10.1039/d0nj02969f

rsc.li/njc

Manipulating the emission characteristics of phosphors is a viable strategy to produce unique, and thus difficult to replicate, security optical features that are useful in anticounterfeiting applications. Here, a fluorophore, BODIPY 493/503, displayed altered solid-state emission characteristics upon being hosted within a crystalline molecular flask. Specifically, a bathochromic shift of 939 cm^{-1} was observed ($\lambda_{(max)}$: 633 → 673 nm), with a concomitant reduction in emission intensity, and emission dependency on excitation wavelength. Multiple factors likely contribute to this behaviour, such as emission filtering by the host framework, exciplex formation between BODIPY and the electron-deficient framework, and collisional quenching between the host and guest. Here we prioritize solid-state analyses to explore these factors, including electron density mapping of the framework pores, and multinuclear solid-state NMR spectroscopy.

Introduction

Optical security features are a relatively common addition to valuable items (*e.g.* high-denomination currencies), and important documents (*e.g.* passports, licenses, certificates), as a means of quickly identifying counterfeits. In response to these inclusions, forgeries have grown in sophistication prompting a need to develop new solid-state security features that are more difficult to replicate. One strategy to achieve this while retaining the existing gamut of emissive dyes is to exert control over their emission profile, thereby tailoring unique, and challenging to replicate, optical outputs. Given the growing prevalence of devices like multi- and hyper-spectral imaging cameras in commercial settings that are capable of quickly and accurately assessing a material's optical signatures, there is a growing market for bespoke optical materials and luminescent labels with unique emission profiles. We propose hosting emissive dyes within a porous framework as a means of manipulating their emission characteristics by harnessing host–guest interactions, and filtering guest emissions through the host framework.

Among the porous host candidates for fluorophores, crystalline sponges show particular promise owing to their structural flexibility and established protocols for guest loading.[1,2] Crystalline sponges, $[(ZnI_2)_3(tpt)_2]\cdot x(solvent)$, are 3D framework materials in which chloroform or cyclohexane is the solvent, and tpt corresponds to the tripodal linker 2,4,6-tris(4-pyridyl)-1,3,5-triazine.[3] Upon immersion of an activated framework within a solution of a suitable guest, displacement of exchangeable solvent by a guest occurs with varying degrees of guest ordering. Ordering of guests within the crystalline sponge pores is best achieved by matching the available interactions of the framework, typically π–π interactions,[4] and by matching the size and shape of the guest to the approximate dimensions of the host pores. The crystalline sponge method has been applied in this way to successfully visualize of a range of chemical processes crystallographically, including: thio-Michael additions,[5] cyclisations,[6] amide formation,[7] and Diels–Alder reactions,[8] as well as the structural elucidation of natural products[9] and organic guests,[10] lending credence to the idea of hosting a versatile range of fluorophores within their pores.

There are few reported examples of systems wherein emissive organic guests have been hosted within metal–organic frameworks (MOFs). Representative instances include an organic laser dye hosted within either a stilbene-based MOF or IRMOF-8, and a range of frameworks hosting azobenzenes,[11] stilbenes,[12] and phenyloxazoles.[13] Hosting emissive compounds within a framework, as opposed to the ligands of the framework bearing fluorescent tags, could improve versatility, synthetic ease and

[a] *School of Environment and Science, Griffith University, 170 Kessels Road, Brisbane, QLD 4111, Australia. E-mail: W.Gee@griffith.edu.au*
[b] *School of Physical Sciences, University of Kent, Canterbury, Kent, CT2 7NH, UK*
[c] *School of Chemistry and EaStCHEM, University of St Andrews, North Haugh, St Andrews KY16 9ST, UK*
[d] *Department of Chemistry, University of Bath, Claverton Down, Bath, BA2 7AY, UK. E-mail: a.d.burrows@bath.ac.uk*

† Electronic supplementary information (ESI) available: Details of synthesis and characterisation, a comparison of PXRD and IR data pre- and post-guest inclusion, and additional multinuclear NMR data. Crystallographic data (CIF) supporting information (PDF). See DOI: 10.1039/d0nj02969f

enable the rapid screening of many fluorophores using a single host system. Applying an activated crystalline sponge to a mixture of multiple luminophores is a potential route to multimodal emissive materials, further enhancing the difficulty of replicating the emission profile of an optical solid-state material in an anticounterfeiting context. Despite crystalline sponge systems being well suited to hosting small molecules, no luminescence studies of emissive guests in these systems have been reported to our knowledge. The potential for such activity can however be inferred from a past report of a hosted thermochromic guest that was capable of switching between conformers using UV radiation (λ = 366 nm).[14] It should be noted that a distinction is made here between porous materials that through design may be loaded with dyes, and dye inclusion crystals, in which the included dye is incorporated during the crystal growth phase in a concentration in the order of 1 part per 10^3–10^6.[15] Similarly, tuning fluorescent emission in MOFs by varying the identity or occupancy of an emissive metal center,[16] *e.g.* lanthanides MOFs, is treated here as a separate topic.

To showcase the manipulation of guest emission by hosting within a porous framework, a single commercial dye, BODIPY 493/503 (abbreviated to BODIPY hereafter), was herein hosted within a crystalline sponge, $[(ZnI_2)_3(tpt)_2]\cdot x(C_6H_{12})$ (**1**), and its optical characteristics compared to solid-state BODIPY to observe changes in its emission profile. BODIPY incorporation into materials is integral to several applications, including tunable lasers sources,[17] biological sensors,[18] and photocatalysts.[19] Interestingly, a relationship linking the extent of BODIPY aggregation in solution to emission profile has recently been established.[20] Here, crystallographic studies and solid-state NMR spectroscopy provide insights regarding the dye's local environment, degree of aggregation, and other influences that a porous framework imparts over a hosted emissive guest.

Experimental

General considerations

Starting materials and solvents were purchased from commercial sources and used as received. The synthesis and matching of characterization for the crystalline sponge ligand tpt[21] and the synthesis of the 'empty' framework followed by loading of the pores with cyclohexane[3b,22] were both carried out following published protocols. Solution phase NMR spectra were recorded either on a Bruker Advance 300 MHz Ultrashield NMR spectrometer or a 500 MHz Bruker Advance II+ NMR spectrometer. Infrared spectra were recorded on a PerkinElmer Spectrum 100 spectrometer equipped with an ATR sampling accessory. Abbreviations for IR bands are s = strong, m = medium, w = weak, br = broad. Elemental analyses (CHN) were performed on a CE-440-Elemental Analyzer (Exeter Analytical). Solid-state UV-vis reflectance spectrometry of powder samples over 250–900 nm was conducted using a PerkinElmer Lambda 750 s UV/Vis/NIR spectrophotometer fitted with a Labsphere 60 mm integrating sphere. Background correction was performed using a Labsphere certified reflectance standard. Solid-state fluorescence measurements were obtained using a LS 55 Luminescence Spectrometer (PerkinElmer).

Synthesis of crystalline sponge-BODIPY material

Single crystals of crystalline sponge **1** were activated by exchange of the solvents of synthesis (nitrobenzene, methanol) with cyclohexane according to a previously reported method.[3b,22] These activated crystals were then suspended in a concentrated green solution of BODIPY dissolved in cyclohexane. After one week the formerly colorless crystals had adopted an orange hue giving **1**·BODIPY of composition $[(ZnI_2)_3(tpt)_2]\cdot 0.65BODIPY\cdot 1.2C_6H_{12}$.

1·BODIPY

FTIR $\bar{\nu}$ = 2922 (m), 2848 (m), 1619 (w), 1576 (w), 1516 (s), 1448 (w), 1422 (w), 1374 (s), 1314 (m), 1234 (s), 1126 (m), 1059 (s), 1025 (m), 982 (m), 867 (w), 802 (s), 748 (w), 668 (m), 655 (s) cm^{-1}. $[(ZnI_2)_3(tpt)_2]\cdot 0.65BODIPY\cdot 1.2C_6H_{12}$ $C_{calc.}$: 33.89, C_{found}: 33.71, $H_{calc.}$: 2.69, H_{found}: 2.68, $N_{calc.}$: 10.05, N_{found}: 10.01.

Crystallographic data

The electron density map of **1**·BODIPY was generated from single crystal X-ray data obtained with an Agilent SuperNova diffractometer using Cu(Kα) radiation. The analysis was conducted at 150 K. The structure was solved using SHELXS-97 and refined using full-matrix least squares in SHELXL-97.[23] The electron density map was generated using Olex2.[24] Despite the crystals diffracting well when irradiated with X-rays, the BODIPY guest did not exhibit a degree of ordering within the pores of the crystalline sponge that allowed unambiguous assignment of its structure. Consequently, the obtained crystallographic data offers little insight beyond the electron density map discussed below. **1**·BODIPY: $C_{39}H_{30}I_6N_{12}Zn_3$ (M = 1624.26 g mol^{-1}): monoclinic, space group $C2/c$ (no. 15), crystal size: 0.1785 × 0.101 × 0.0678 mm^3, a = 35.2899(10) Å, b = 14.8461(3) Å, c = 32.3685(9) Å, β = 103.634(3)°, V = 16480.5(8) $Å^3$, Z = 8, ν = 18.867 mm^{-1}, $D_{calc.}$ = 1.309 g cm^{-3}, 29 531 reflections measured (6.488° ≤ 2Θ ≤ 117.862°), 11 822 unique (R_{int} = 0.0325, R_{Sigma} = 0.0318) which were used in all calculations. The final R_1 was 0.0953 ($I > 2\sigma(I)$) and wR_2 was 0.3443 (all data). CCDC 1535880.

Solid-state NMR data

Solid-state NMR spectra were recorded on a Bruker Advance II spectrometer equipped with a 9.4 T wide-bore superconducting magnet, yielding Larmor frequencies of 400.1 MHz for ^{1}H, 128.4 MHz for ^{11}B, 100.6 MHz for ^{13}C and 376.4 MHz for ^{19}F. Samples were packed into 1.9 mm (BODIPY and **1**·BODIPY) or 4 mm (**1**) zirconia rotors and rotated at the magic angle at 40 kHz (^{1}H), 30 kHz (^{19}F), 33.33 kHz (^{11}B) or 12.5 kHz (^{13}C). The ^{11}B–^{19}F heteronuclear correlation spectrum was recorded with magic angle spinning (MAS) at a rate of 25 kHz.

^{1}H and ^{19}F NMR spectra were recorded with a rotor-synchronized spin echo pulse sequence, using an echo delay of one rotor period to remove the probe background signal. For ^{1}H, 16 transients were averaged with a recycle interval of 10 s. For ^{19}F, 128 transients were averaged with a recycle interval of 10 s. ^{11}B NMR spectra were recorded using a rotor-synchronized

spin echo sequence to remove the probe background and with rotor-synchronized π-pulse decoupling of ^{19}F ($\nu_1 \sim 83$ kHz) applied during acquisition to improve spectral resolution. 128 (BODIPY) or 256 (**1**·BODIPY) transients were averaged with a recycle interval of 10 s. ^{13}C NMR spectra were recorded with cross polarization (CP) from ^{1}H to improve sensitivity. A contact pulse (ramped from 90–100% for ^{1}H) duration of 1.5 ms was used and TPPM-15 decoupling of ^{1}H ($\nu_1 \sim 83$ kHz) was applied during acquisition. 5120 (BODIPY), 16 384 (**1**·BODIPY) or 512 (**1**) transients were averaged with a recycle interval of 3 s. The two-dimensional ^{11}B–^{19}F NMR spectrum was recorded with the refocused INEPT pulse sequence. Signal averaging was carried out for 768 transients with a recycle interval of 3 s for each of 12 t_1 increments of 20 μs. Rotor-synchronized π-pulse decoupling of ^{19}F ($\nu_1 \sim 83$ kHz) was applied during acquisition.

Results and discussion

Before assessing the optical properties of BODIPY hosted within framework **1**, detailed characterization of the host–guest material was first undertaken. The structure of both framework **1** and the BODIPY dye used in this study are shown in Fig. 1. After activation, single crystals of **1** were suspended in a characteristic green solution of concentrated BODIPY in cyclohexane for a period of one week. During this time the crystals changed colour from a slight yellow hue to vivid orange, demonstrating uptake of the fluorophore by the host to yield **1**·BODIPY. To ascertain whether the framework motif was retained post-guest uptake, powder X-ray diffraction (PXRD) and infrared (IR) analyses were performed on frameworks **1** and **1**·BODIPY. Both experimental PXRD patterns compared favorably to the calculated pattern for the cyclohexane-loaded crystalline sponge (Fig. S1, ESI†). Each pattern appears closely related, reflecting similar framework topologies despite the dissimilar nature of the hosted BODIPY guest relative to the pre-loaded cyclohexane solvent. Next the guest, crystalline BODIPY, was measured in the absence of the host, which revealed that the powder patterns shared no similar peaks with **1**·BODIPY (Fig. S2, ESI†). This suggests that BODIPY molecules are hosted within the framework pores rather than forming a polycrystalline coating on the surface of the host.

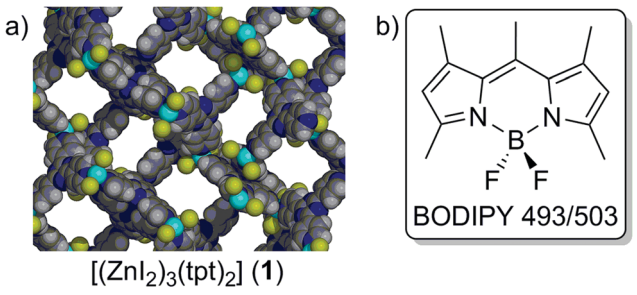

Fig. 1 (a) Framework **1** viewed down the crystallographic *b* axis highlighting a network of channels capable of hosting guest molecules. (b) Chemical structure of the guest, BODIPY 493/503, which is referred to as BODIPY in this study.

Comparison of the IR carbonyl regions of **1** and **1**·BODIPY revealed matching features, including retention of all prominent bands in the fingerprint region (Fig. S3 and S4, ESI†). New bands were observed in the aromatic region for **1**·BODIPY, including strong vibrations at 1235, 1126 and 983 cm^{-1}. The latter two bands can be attributed to B–F stretching vibrations,[25] which provide further evidence for inclusion of BODIPY within **1**, whereas the former band is tentatively attributed to C–N stretching vibrations from the BODIPY scaffold.

Next, single crystals of **1**·BODIPY were analysed crystallographically to visualize guest behaviour within the framework pores. Analysis of a well-diffracting crystal that exhibited sharp diffraction peaks yielded a framework structure that was unchanged from **1** post inclusion of BODIPY. In addition, residual electron density modelled within the framework pores identified a molecular species that matched the expected size and profile of the BODIPY molecule (Fig. S5 and S6, ESI†). This data enabled assignment of the likely location of the guest within **1**·BODIPY, however the precise orientation of that guest could not be unambiguously determined. BODIPY and tpt are both aromatic systems that each possess an electron deficient character, meaning that parallel π–π interactions between the two are not favoured.[26] This repulsive force inhibits the guest-ordering potential of π-interactions between tpt and BODIPY, contrasting with the behaviour expected from electron-rich aromatic guests. This is highlighted by the longer inter-planar distance of 3.66 Å between the central tpt ring and the mean plane defined by the residual electron density peaks attributable to BODIPY, which compares to 3.4 Å for triphenylene when analogously hosted within the same crystalline sponge motif.[27] Consequently, diffuse B–F···tpt interactions that are poorly suited to imparting long-range ordering predominate in **1**·BODIPY.

Determination of the loading ratio of BODIPY was achieved by washing a crystalline sample (5–10 single crystals) of **1**·BODIPY with chloroform, followed by air-drying and digestion of the sample in DMF-d_7 for analysis by ^{1}H-NMR spectroscopy. The spectrum of digested **1**·BODIPY (Fig. 2) showed pyrromethene resonances consistent with BODIPY,[28] which have been assigned below. Comparing the integrals of the aromatic proton resonance of BODIPY, labelled 2 in Fig. 2, with an aromatic resonance of tpt results in a ratio of 1 : 3.08 (BODIPY : tpt). Crystallographic studies determined that the asymmetric unit of **1** contains two unique tpt ligands (Fig. S5, ESI†), hence the ^{1}H-NMR integral ratio suggests a loading value of 0.65 equivalents of BODIPY per formula unit, or $[(ZnI_2)_3(tpt)_2]\cdot 0.65$BODIPY. It should be noted that the intensity of the ^{1}H-NMR data in Fig. 2 is low. This is because the data was sourced from a digested sample of **1**·BODIPY derived from a small, single crystalline batch of **1** wherein crystallisation had been halted upon the first appearance of single crystals. **1**·BODIPY sourced in this manner yielded superior characterisation data relative to larger batches of **1**, or instances wherein extended crystal growth periods were allowed. However, this approach suffers from the disadvantage of limited availability of materials for analysis, giving rise to the observed low signal-to-noise ratio. Calculating integral ratios from low intensity NMR data introduces uncertainty that is

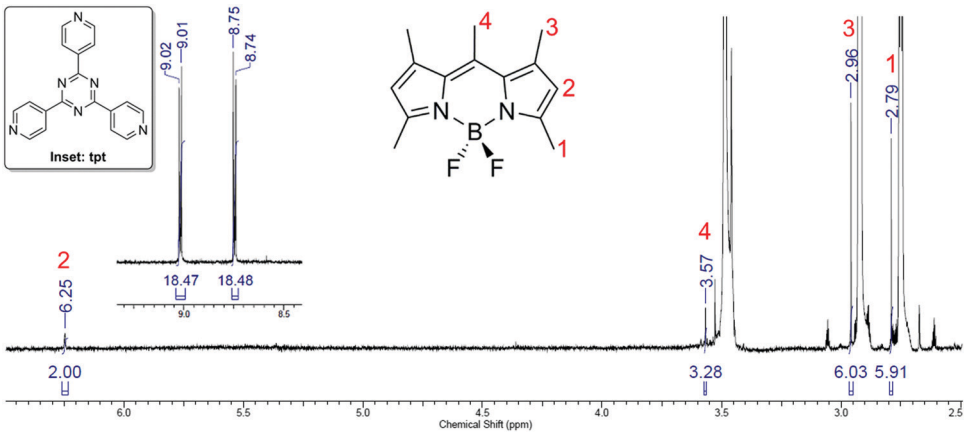

Fig. 2 ^{1}H-NMR spectrum obtained from digested single crystals of **1**·BODIPY in DMF-d_7. Peaks corresponding to BODIPY are numbered in red, and the inset spectrum shows the aromatic residues of the ligand tpt used for calculating the integral ratio.

carried forward to the calculation of loading values. Next, a ^{1}H-NMR spectrum was obtained from a large (*ca.* 3 × 1 × 1 mm) individual single crystal of **1**·BODIPY digested in DMF-d_7 (Fig. S7, ESI†). While the issue of low signal intensity persisted, clear evidence of both tpt and BODIPY were obtained from the single crystal. The sample yielded a loading value of 0.46 equivalents of BODIPY per crystallographic formula unit as determined from the ^{1}H-NMR integral ratios. The decrease in guest loading determined for the individual crystal relative to the multi-crystal sample may be due to the decreased surface area to volume ratio for the large single crystal. This could inhibit solvent exchange during activation of **1**, as well as the uptake of BODIPY during the subsequent loading phase. Notably, very large single crystals were unsuited to crystallographic analysis owing to the prevalence of crystal defects. Such defects could block the channels within the crystalline sponge, making larger single crystals less amenable to guest inclusion and giving rise to the reduced loading value.

A ^{19}F-NMR spectrum was also performed on the digestion product, yielding a sharp 1 : 1 : 1 : 1 quartet at −145.5 ppm (Fig. S8, ESI†) attributed to the BF_2 group of BODIPY. The elemental analysis data for a dried sample of **1**·BODIPY matches an elemental composition of $[(ZnI_2)_3(tpt)_2]$·0.65BODIPY·1.2C_6H_{12} with C, 33.71 (predicted: 33.89), H, 2.68 (2.69), and N, (10.01 (10.05)). This is consistent with the ^{1}H-NMR data for **1**·BODIPY given the propensity of cyclohexane to desolvate from the pores of crystalline sponge materials upon drying.

Solid-state NMR spectroscopy provided additional evidence of host–guest interactions between BODIPY and framework **1**. ^{1}H-MAS-NMR spectra (Fig. S9, ESI†) confirmed the dye to be present within the framework, and that hosted BODIPY undergoes dynamic processes within the framework pores based on the much sharper resonances observed for the CH_3 groups relative to the bulk dye. This highlights the conformational freedom provided to BODIPY when hosted in the porous framework that is absent in the solid-state crystalline BODIPY. The ^{11}B-MAS-NMR spectra (Fig. 3(a)) confirmed the presence of a tetrahedral boron atom in both materials, with a small upfield shift of 0.3 ppm in **1**·BODIPY suggesting a slightly increased electron density on the boron upon loading into the crystalline sponge. ^{13}C-CPMAS-NMR spectra (Fig. S10, ESI†) also confirmed the inclusion of BODIPY into the framework, but were unable to provide further insight into the nature of the host–guest interactions. ^{19}F-MAS-NMR spectroscopy (Fig. 3(b)) showed the presence of a single resonance at −144.6 ppm for the bulk BODIPY, but three resonances at −142.2, −146.0 and −147.1 ppm in **1**·BODIPY. These three resonances exhibited a reduced chemical shift anisotropy relative to the bulk material, suggesting again that the BODIPY is more dynamic within the crystalline sponge than in the bulk solid. A further resonance was observed at −81.9 ppm in the ^{19}F-NMR spectrum of **1**·BODIPY. A through-bond ^{11}B–^{19}F heteronuclear correlation spectrum (Fig. 3(c)) shows that the fluorine species responsible for this resonance is not bonded to boron, suggesting that, over time, a fluoride/iodide exchange may take place between the BODIPY and the framework. This assertion is consistent with the crystallographically determined location of the guest within **1**·BODIPY proximal to iodide at the ZnI_2 metal nodes, as well as the slightly enhanced amount of observed electron density at the fluoride location oriented towards the ZnI_2, which may be indicative of a small degree of iodine substitution.

With the degree of guest loading established and an approximate location of **1** within the pore discerned, solid-state luminescence characterization of **1**·BODIPY was undertaken. Viewing **1**, **1**·BODIPY and BODIPY, under both white light and ultraviolet radiation (λ_{ex} = 253 nm, 365 nm) provided an initial assessment of each material's luminescent behaviour (Fig. 4). It is worth noting that BODIPY emits red light when ordered in the solid state (Fig. 4(a)), but green light when dissolved in solution.[17–19] The emission behaviour of **1**·BODIPY is interesting given that the pore environment of the framework should offer BODIPY more dynamic freedom than it experiences in its neat crystalline form, yet considerably greater ordering than when it is dissolved in solution. As seen in Fig. 4, a crystalline powder of **1** appears pale yellow under white-light illumination, while BODIPY appears red, and **1**·BODIPY appears orange. Under UV irradiation, BODIPY is emissive when excited by both 365 and 253 nm wavelengths, whereas the empty

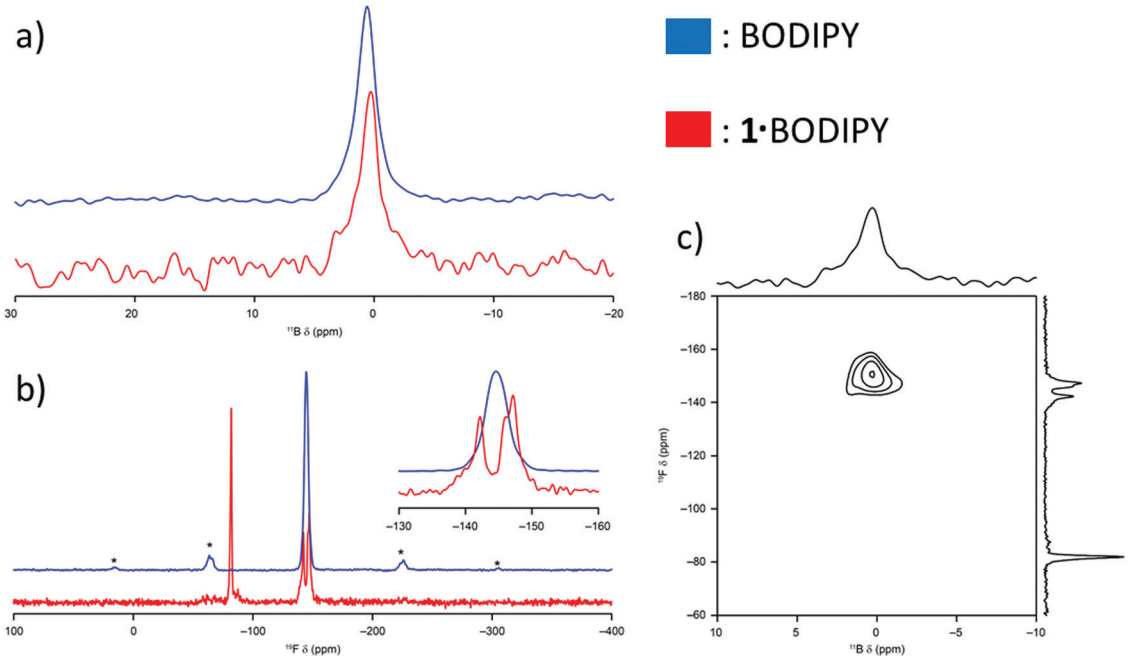

Fig. 3 (a) ^{11}B (9.4 T, 33.33 kHz MAS) NMR spectra of BODIPY (blue) and **1**·BODIPY (red). (b) ^{19}F (9.4 T, 30 kHz MAS) NMR spectra of BODIPY (blue) and **1**·BODIPY (red). Asterisks indicate spinning sidebands arising from the chemical shift anisotropy and the inset shows an expansion of the region from −130 to −160 ppm. (c) ^{11}B–^{19}F (9.4 T, 25 kHz MAS) refocused INEPT correlation spectrum of **1**·BODIPY. The ^{11}B- and ^{19}F-MAS-NMR spectra are shown along the respective axes for comparison.

framework **1** exhibits no observable fluorescent emissions. The host–guest material, **1**·BODIPY, yielded no discernible emission at an excitation wavelength of 365 nm (Fig. 4(b)), yet at 253 nm low intensity red-shifted fluorescence was visible (Fig. 4(c)). This red emission signifies that when hosted within the pores of **1**, BODIPY adopts emission behaviour reminiscent of the solid state as opposed to the solution state. It is worth noting that both crystalline BODIPY and **1**·BODIPY were irradiated at known optimal wavelengths for triggering fluorescent emission in solution (λ = 430, 520 nm),[16–18] however these yielded no detectable solid-state emissions.

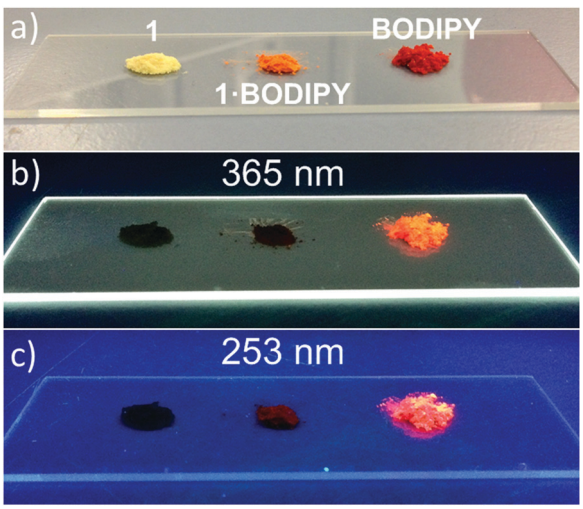

Fig. 4 (a) From left to right, powdered samples of $[(ZnI_2)_3(tpt)_2]\cdot x(C_6H_{12})$ (**1**), crystalline sponge hosting BODIPY (**1**·BODIPY), and crystalline BODIPY. (b) Orange emission from solid BODIPY under irradiation from 365 nm radiation. (c) Weak red emission from **1**·BODIPY and strong orange emission from BODIPY when irradiated by 253 nm radiation. No fluorescent emission from crystalline sponge **1** was detected for either UV wavelength.

The UV-visible diffuse-reflectance spectroscopy (DRS) profile of powdered **1** (Fig. 5, blue trace) and BODIPY (Fig. 5, green trace) were next characterized. This analysis revealed that the framework and the guest both absorb strongly in the UV region, after which the absorption profile of framework **1** sharply declines across the range of 400 nm to 475 nm, before tailing to virtually no absorption above 700 nm. BODIPY absorbs light up to 550 nm, then exhibits a decrease in absorption as observed for **1**, albeit retaining some absorptivity up to and beyond 900 nm.

Fluorescence measurements were performed on crystalline BODIPY, as to our knowledge, no prior reports of solid-state emission characteristics are available for this fluorophore. Other structurally similar BODIPY fluorophores have been shown to generate analogous red solid-state emissions.[29] The fluorescent emission for BODIPY (Fig. 5, red trace) features a $\lambda_{(max)}$ at 633 nm, and ranges from 590 to 730 nm resembling a slightly skewed Gaussian distribution. Optimization of the excitation wavelength was performed by comparing emission intensity at the $\lambda_{(max)}$ across a range of excitation wavelengths (Fig. 5, inset). This showed 253 nm to be near to the optimal excitation wavelength for triggering fluorescent emissions from BODIPY. Consequently, this excitation wavelength was used for all subsequent fluorescent measurements of **1**·BODIPY. The emission of **1**·BODIPY was found to be *ca.* 40 times less intense than for crystalline BODIPY and showed a red-shift of 939 cm^{-1} ($\lambda_{(max)}$ = 673 nm), however direct comparison would be

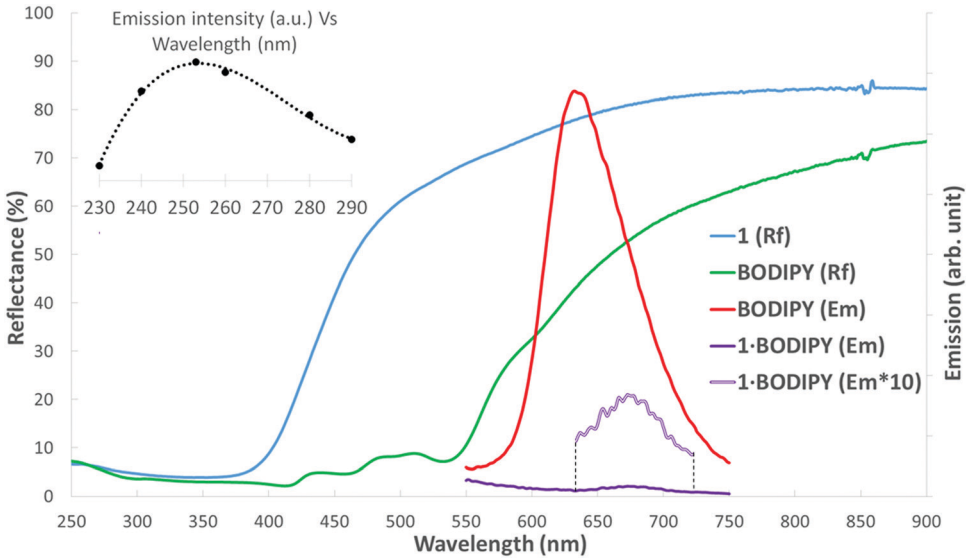

Fig. 5 Reflectance spectrum of empty **1** (blue) and BODIPY (green) plotted alongside the normalized emission spectra of BODIPY (red) and **1**·BODIPY (solid purple). To account for the difference in relative abundance of fluorophore (*vide infra*) in pure BODIPY and **1**·BODIPY, the intensity of purple spectrum has been amplified by 10× (open purple). The increasing signal trend for **1**·BODIPY from <600 nm derives from a second-order transmission artefact.

misleading given the differences in relative abundance of the fluorophore present in each sample. From crystallographic insights and spectroscopic determination of guest loading in **1**·BODIPY, it can be inferred that the sample contains 10.2% fluorophore by volume, compared with 100% for neat crystalline BODIPY (see ESI,† for further discussion).[20b] To account for this difference in relative fluorophore abundance, a tenfold enhancement was applied to the emission of **1**·BODIPY, shown as the broken purple trace in Fig. 5.

Adjusting for the differences in the fluorophore ratio, the fluorescent emission intensity of **1**·BODIPY is quenched by approximately 80% relative to BODIPY, concomitant with an apparent bathochromic shift. A combination of factors likely accounts for these observations, however we propose that the crystalline sponge may act as an innate filter for emissions deriving from the BODIPY guest. One indication of this is that **1**·BODIPY emits only at 253 nm, whereas non-hosted BODIPY can emit at both 253 and 365 nm, suggesting that framework **1** effectively screens the latter excitation wavelength from the guest. This change in behaviour to selective emission triggered by a specific wavelength is useful in the context of creating a difficult to replicate anticounterfeiting material.[30] The reflectance profile for **1** also shows a tailing absorption trend covering the entirety of the BODIPY emission region (590–730 nm, Fig. 5) that would provide a more pronounced filtering effect at shorter wavelengths, thereby selectively transmitting the longer wavelengths of BODIPY emission. This provides one possible explanation for the apparent shift of the hosted BODIPY emission maximum to 673 nm, coupled with a decline in overall emission intensity. However, an alternate explanation for this behaviour cannot be excluded, that being quenching resulting from exciplex formation between hosted BODIPY and a tpt ligand of the $[(ZnI_2)_3(tpt)_2]$ framework, given the location and cofacial orientation of BODIPY over a tpt ligand (3.66 Å) (Fig. S5, ESI†). It is known that in frameworks where chromophores are confined in close proximity that formation dynamics of exciplexes may be very fast, and for solid-state samples this depends on the local concentration of the chromophores, and their relative orientation.[31] Exciplex formation is an alternate explanation for bathochromic shifting of fluorescent emission, however such behaviour typically requires strong host–guest interactions between guest and framework. This has been observed in porous frameworks comprised of functionalized anthracene ligands when hosting aniline analogues and was attributed to charge-transfer interactions upon exciplex formation.[32] Indeed tuneable bathochromic shifts were reported for BODIPY molecules that were co-encapsulated with various polyaromatic guests analogous to tpt.[33] Finally, a third cause of quenching also cannot be discounted; iodide is a component of the ZnI_2 metal nodes which are oriented towards the BODIPY guest as determined by the solid-state characterization data. This implies that the metal nodes of framework **1** may be well-positioned to act as a collisional quencher of guest emissions.[34]

Using host–guest chemistry to alter the optical properties of a common dye, shown here by imparting wavelength-dependent emission behaviour and shifted emission colour, are both interesting outcomes from the perspective of developing new anticounterfeiting materials from known luminophores. Herein we have identified the probable factors influencing the emission profile of a hosted BODIPY dye, those being the optical absorption properties of the framework, exciplex formation, and possible collisional quenching between the framework and guest. By focusing on solid-state characterization methods, these findings have been made applicable to common solid phase manufactured anticounterfeiting products such as emissive security labels, and other optical security features. Frameworks such as crystalline sponges represent a useful system for investigating such effects with emphasis on identifying solid-state interactions,

as accessible and ordered pore networks provide opportunities to infer host–guest interactions involving the fluorophore, and thus its emission, post-synthesis.

Conclusions

In conclusion, we have evaluated the solid-state fluorescence of BODIPY and the influence that hosting within a crystalline sponge has on that emission. Bathochromic shifting of fluorescent emission was observed, which has been attributed to optical filtering from the framework, however the possibility of exciplex formation between BODIPY and the framework ligand tpt cannot be excluded. These assertions are evidenced by multinuclear solid-state NMR spectroscopy, which identified small shifts in peak positions indicating an interaction between BODIPY and the crystalline sponge, as well as a difference electron density map of the pores of **1**·BODIPY, and solid-state fluorescence studies. The UV-visible diffuse-reflectance spectrum of **1** shows that emission wavelengths below 450 nm will be strongly absorbed, with this effect lessening up to *ca.* 650 nm. This suggests crystalline sponges are best suited to hosting fluorophores that primarily emit beyond 650 nm and may alter the emission profile of guests by imparting a filter effect. These results provide interesting insights that will assist with the development of new solid-state emissive materials with potential use in anticounterfeiting applications.

Author contributions

The manuscript was written through contributions of all authors. All authors have given approval to the final version of the manuscript.

Abbreviations

BODIPY	Boron-dipyrromethene
IR	Infrared
MAS	Magic angle spinning
MHz	Megahertz
MOF	Metal–organic framework
NMR	Nuclear magnetic resonance
PXRD	Powder X-ray diffraction
tpt	2,4,6-Tris(4-pyridyl)-1,3,5-triazine
UV/Vis/NIR	Ultraviolet/visible/near infrared

Conflicts of interest

The authors declare no competing financial interests.

Acknowledgements

The authors gratefully acknowledge support from an EPSRC programme grant (grant no. EP/K004956/1).

References

1 Y. Inokuma, M. Kawano and M. Fujita, Crystalline molecular flasks, *Nat. Chem.*, 2011, **3**, 349–358.
2 (*a*) Y. Inokuma, S. Yoshioka, J. Ariyoshi, T. Arai and M. Fujita, Preparation and guest-uptake protocol for a porous complex useful for 'crystal-free' crystallography, *Nat. Protoc.*, 2014, **9**, 246–252; (*b*) T. R. Ramadhar, S.-L. Zheng, Y.-S. Chen and J. Clardy, Analysis of rapidly synthesized guest-filled porous complexes with synchrotron radiation: practical guidelines for the crystalline sponge method, *Acta Crystallogr., Sect. A: Fundam. Crystallogr.*, 2015, **71**, 46–58.
3 (*a*) Y. Inokuma, S. Yoshioka, J. Ariyoshi, T. Arai, Y. Hitora, K. Takada, S. Matsunaga, K. Rissanen and M. Fujita, X-ray analysis on the nanogram to microgram scale using porous complexes, *Nature*, 2013, **495**, 461–466; (*b*) Y. Inokuma, S. Yoshioka, J. Ariyoshi, T. Arai, Y. Hitora, K. Takada, S. Matsunaga, K. Rissanen and M. Fujita, Corrigendum: X-ray analysis on the nanogram to microgram scale using porous complexes, *Nature*, 2013, **501**, 262; (*c*) M. Hoshino, A. Khutia, H. Xing, Y. Inokuma and M. Fujita, The crystalline sponge method updated, *IUCrJ*, 2016, **3**, 139–151; (*d*) W. J. Gee, The growing importance of crystalline molecular flasks and the crystalline sponge method, *Dalton Trans.*, 2017, **46**, 15979–15986.
4 O. Ohmori, M. Kawano and M. Fujita, Construction of biporous coordination networks *via* π–π interaction, *CrystEngComm*, 2005, **7**, 255–259.
5 V. Duplan, M. Hoshino, W. Li, T. Honda and M. Fujita, In Situ Observation of Thiol Michael Addition to a Reversible Covalent Drug in a Crystalline Sponge, *Angew. Chem., Int. Ed.*, 2016, **55**, 4919–4923.
6 J. V. Knichal, H. J. Shepherd, C. C. Wilson, P. R. Raithby, W. J. Gee and A. D. Burrows, An Iodine-Vapor-Induced Cyclization in a Crystalline Molecular Flask, *Angew. Chem., Int. Ed.*, 2016, **55**, 5943–5946.
7 W. J. Gee, L. K. Cadman, H. Amer Hamzah, M. F. Mahon, P. R. Raithby and A. D. Burrows, Furnishing Amine-Functionalized Metal–Organic Frameworks with the β-Amidoketone Group by Postsynthetic Modification, *Inorg. Chem.*, 2016, **55**, 10839–10842.
8 K. Ikemoto, Y. Inokuma and M. Fujita, Diels–Alder *via* molecular recognition in a crystalline molecular flask, *J. Am. Chem. Soc.*, 2011, **133**, 16806–16808.
9 Y. Inokuma, T. Ukegawa, M. Hoshino and M. Fujita, M. Structure determination of microbial metabolites by the crystalline sponge method, *Chem. Sci.*, 2016, **7**, 3910–3913.
10 E. V. Vinogradova, P. Müller and S. L. Buchwald, Structural Reevaluation of the Electrophilic Hypervalent Iodine Reagent for Trifluoromethylthiolation Supported by the Crystalline Sponge Method for X-ray Analysis, *Angew. Chem., Int. Ed.*, 2014, **53**, 3125–3128.
11 N. Yanai, T. Uemura, M. Inoue, R. Matsuda, T. Fukushima, M. Tsujimoto, S. Isoda and S. Kitagawa, Guest-to-Host Transmission of Structural Changes for Stimuli-Responsive Adsorption Property, *J. Am. Chem. Soc.*, 2012, **134**, 4501–4504.

12 (*a*) D. Yan, Y. Tang, H. Lin and D. Wang, Tunable Two-color Luminescence and Host–guest Energy Transfer of Fluorescent Chromophores Encapsulated in Metal-Organic Frameworks, *Sci. Rep.*, 2014, **4**, 4337–4344; (*b*) N. Yanai, K. Kitayama, Y. Hijikata, H. Sato, R. Matsuda, Y. Kubota, M. Takata, M. Mizuno, T. Uemura and S. Kitagawa, Gas detection by structural variations of fluorescent guest molecules in a flexible porous coordination polymer, *Nat. Mater.*, 2011, **10**, 787–793.

13 (*a*) D. Yan, G. O. Lloyd, A. Delori, W. Jones and X. Duan, Tuning Fluorescent Molecules by Inclusion in a Metal–Organic Framework: An Experimental and Computational Study, *ChemPlusChem*, 2012, **77**, 1112–1118; (*b*) R. Grünker, V. Bon, A. Heerwig, N. Klein, P. Müller, U. Stoeck, I. A. Baburin, U. Mueller, I. Senkovska and S. Kaskel, Dye Encapsulation Inside a New Mesoporous Metal–Organic Framework for Multifunctional Solvatochromic-Response Function, *Chem. – Eur. J.*, 2012, **18**, 13299–13303.

14 T. Haneda, M. Kawano, T. Kojima and M. Fujita, Thermo-to-Photo-Switching of the Chromic Behavior of Salicylideneanilines by Inclusion in a Porous Coordination Network, *Angew. Chem., Int. Ed.*, 2007, **46**, 6643–6645.

15 B. Kahr and R. W. Gurney, Dyeing Crystals, *Chem. Rev.*, 2001, **101**, 893–951.

16 (*a*) W. Huang, F. Pan, Y. Liu, S. Huang, Y. Li., J. Yong, Y. Li, A. M. Kirillov and D. Wu, An Efficient Blue-Emissive Metal–Organic Framework (MOF) for Lanthanide-Encapsulated Multicolor and Stimuli-Responsive Luminescence, *Inorg. Chem.*, 2017, **56**, 6362–6370; (*b*) J. An, C. M. Shade, D. A. Chengelis-Czegan, S. Petoud and N. L. Rosi, Zinc-Adeninate Metal-Organic Framework for Aqueous Encapsulation and Sensitization of Near-infrared and Visible Emitting Lanthanide Cations, *J. Am. Chem. Soc.*, 2011, **133**, 1220–1223.

17 T. G. Pavlopoulos, J. H. Boyer, K. Thangaraj, G. Sathyamoorthi, M. P. Shah and M.-L. Soong, Laser dye spectroscopy of some pyrromethene-BF_2 complexes, *Appl. Opt.*, 1992, **31**, 7089–7094.

18 G. Ulrich, R. Ziessel and A. Harriman, The Chemistry of Fluorescent Bodipy Dyes: Versatility Unsurpassed, *Angew. Chem., Int. Ed.*, 2008, **47**, 1184–1201.

19 L. Wang, J. Cao, J.-W. Wang, Q. Chen, A.-J. Cui and M.-Y. He, Facile synthesis of dimeric BODIPY and its catalytic activity for sulfide oxidation under visible light, *RSC Adv.*, 2014, **4**, 14786–14790.

20 (*a*) H. Manzano, I. Esnal, T. Marqués-Matesanz, J. Bañuelos, I. López-Arbeloa, M. J. Ortiz, L. Cerdán, A. Costela, I. García-Moreno and J. L. Chiara, Unprecedented J-Aggregated Dyes in Pure Organic Solvents, *Adv. Funct. Mater.*, 2016, **26**, 2756–2769; (*b*) S. Choi, J. Bouffard and Y. Kim, Aggregation-induced emission enhancement of a *meso*-trifluoromethyl BODIPY *via* J-aggregation, *Chem. Sci.*, 2014, **5**, 751–755.

21 A. Herrera, R. Martínez-Alvarez, P. Ramiro, M. Chioua and R. Chioua, A Practical and Easy Synthesis of 2,4,6-Trisubstituted-*s*-triazines, *Synthesis*, 2004, 503–505.

22 Y. Inokuma, S. Yoshioka, J. Ariyoshi, T. Arai and M. Fujita, Preparation and guest-uptake protocol for a porous complex useful for 'crystal-free' crystallography, *Nat. Protoc.*, 2014, **9**, 246–252.

23 G. M. Sheldrick, A short history of SHELX, *Acta Crystallogr.*, 2008, **A64**, 112–122.

24 O. V. Dolomanov, L. J. Bourhis, R. J. Gildea, J. A. K. Howard and H. Puschmann, *OLEX2*: a complete structure solution, refinement and analysis program, *J. Appl. Crystallogr.*, 2009, **42**, 339–341.

25 R. L. Hunt and B. S. Ault, Spectroscopic influences of ion pairing: Infrared matrix isolation spectra of the M^+BF_{-4} ion pair and its chlorine-fluorine analogs, *Spectrochim. Acta*, 1981, **37A**, 63–69.

26 C. R. Martinez and B. L. Iverson, Rethinking the term ''pi-stacking'', *Chem. Sci.*, 2012, **3**, 2191–2201.

27 O. Ohmori, M. Kawano and M. Fujita, Crystal-to-crystal guest exchange of large organic molecules within a 3D coordination network, *J. Am. Chem. Soc.*, 2004, **126**, 16292–16293.

28 W. Wu, X. Cui and J. Zhao, Hetero Bodipy-dimers as heavy atom-free triplet photosensitizers showing a long-lived triplet excited state for triplet–triplet annihilation upconversion, *Chem. Commun.*, 2013, **49**, 9009–9011.

29 (*a*) H. A. A. El-Ali, J. Jing and X. L. Zhanh, Solid-state emissive O-BODIPY dyes with bimodal emissions across red and near infrared region, *RSC Adv.*, 2019, **9**, 16246–16251; (*b*) Ö. A. Bozdemir, H. H. T. Al-Sharif, W. McFarlane, P. G. Waddell, A. C. Benniston and A. Harriman, Solid-State Emission from Mono- and Bichromophoric Boron Dipyrromethene (BODIPY) Derivatives and Comparison with Fluid Solution, *Chem. – Eur. J.*, 2019, **25**, 15634–15645.

30 G. Truccolo, R. E. Boseley, S. W. Lewis and W. J. Gee, in Forensic applications of lanthanides and rare earths: anticounterfeiting materials and latent fingerprint developers, *Handbook on the Physics and Chemistry of Rare Earths*, ed. J.-C. G. Bünzli and V. K. Pecharsky, Elsevier B.V., Amsterdam, 2020, vol. 58, pp. 1–54.

31 P. Deria, J. Yu, T. Smith and R. P. Balaraman, *J. Am. Chem. Soc.*, 2017, **139**, 5973–5983.

32 D. Tanaka, S. Horike, S. Kitagawa, M. Ohba, M. Hasegawa, Y. Ozawa and K. Toriumi, Anthracene array-type porous coordination polymer with host–guest charge transfer interactions in excited states, *Chem. Commun.*, 2007, 3142–3144.

33 J. R. Lakowicz, *Principles of Fluorescence Spectroscopy*, Springer, 3rd edn, 2010, p. 278.

34 M. Yamashina, M. M. Sartin, Y. Sei, M. Akita, S. Takeuchi, T. Tahara and M. Yoshizawa, Preparation of Highly Fluorescent Host–Guest Complexes with Tunable Color upon Encapsulation, *J. Am. Chem. Soc.*, 2015, **137**, 9266–9269.